ARTICLE IN PRESS

+ MODEL

Available online at www.sciencedirect.com

ScienceDirect

ELSEVIER

Experimental Eye Research xx (2007) 1–11

EXPERIMENTAL EYE RESEARCH

www.elsevier.com/locate/yexer

Predicted extension, compression and shearing of optic nerve head tissues

Ian A. Sigal [a,b,1], John G. Flanagan [c,d], Inka Tertinegg [c], C. Ross Ethier [a,b,c,*]

[a] *Department of Mechanical and Industrial Engineering, University of Toronto, Toronto, Ontario, Canada*
[b] *Institute for Biomaterials and Biomedical Engineering, University of Toronto, Toronto, Ontario, Canada*
[c] *Department of Ophthalmology and Vision Sciences, University of Toronto, Toronto, Ontario, Canada*
[d] *School of Optometry, University of Waterloo, Waterloo, Ontario, Canada*

Received 15 November 2006; accepted in revised form 21 May 2007

Abstract

Glaucomatous optic neuropathy may be in part due to an altered biomechanical environment within the optic nerve head (ONH) produced by an elevated intraocular pressure (IOP). Previous work has characterized the magnitude of the IOP-induced deformation of ONH tissues but has not focused specifically on the mode of deformation (strain), i.e. whether the ONH tissues and cells are stretched, compressed or sheared. Circumstantial evidence indicates that the mode of deformation has biological consequences. Here we use computational models to study the different modes of deformation that occur in an ONH as a result of an increase in IOP. One generic and three individual-specific 3D models of the human ONH were reconstructed as previously described. Each model consisted of five tissue regions: pre and post-laminar neural tissue, lamina cribrosa, sclera and pia mater. Finite element methods were then used to predict the biomechanical response to changes in IOP. For each model we computed six local measures of strain, including the magnitude and direction of maximum stretching, maximum compression and maximum shearing strain. We compared the spatial and population distributions of the various measures of strain by using semi-quantitative (contour plots) and quantitative (histograms) methods. For all models, as IOP increased, the tissues of the ONH were subjected simultaneously to various modes of strain, including compression, extension and shearing. The highest magnitudes of all modes of strain occurred within the neural tissue regions. There were substantial differences in the magnitudes of the various modes of strain, with the largest strains being in compression, followed by shearing and finally by extension. The biomechanical response of an individual-specific ONH to changes in IOP is complex and cannot be fully captured by one measure of deformation. We predict that cells within the ONH are subjected to very different modes of deformation as IOP increases. The largest deformations are compressive, followed by shearing and stretching. Models of IOP-induced RGC damage need to be further refined by characterizing the cellular response to these different modes of strain.

Keywords: glaucoma; optic nerve head; biomechanics; finite elements; strain; compression

1. Introduction

The causes of retinal ganglion cell (RGC) degeneration in glaucoma are still poorly understood, but elevated intraocular pressure (IOP) has been identified as a primary risk factor for the development and progression of glaucomatous optic neuropathy. A biomechanical theory of glaucoma proposes that mechanical effects on the tissues of the optic nerve head (ONH) are, at least in part, responsible for the damaging effects of IOP. Consistent with this theory, it is generally accepted that increases in IOP deform the ONH (Burgoyne et al., 2005; Jonas et al., 2004; Yan et al., 1994), which results in high levels of mechanical strain (Burgoyne et al., 2005; Quigley, 2005; Sigal et al., 2004). Several mechanisms by

* Corresponding author at: Department of Bioengineering, Imperial College, London SW7 2AZ, United Kingdom. Tel./fax: +1 416 978 6728/7753.
E-mail address: ethier@mie.utoronto.ca (C.R. Ethier).
[1] Present address: Ocular Biomechanics Laboratory, Devers Eye Institute, Portland, OR, USA.

0014-4835/$ - see front matter © 2007 Elsevier Ltd. All rights reserved.
doi:10.1016/j.exer.2007.05.005

Please cite this article in press as: Ian A. Sigal et al., Predicted extension, compression and shearing of optic nerve head tissues, Exp. Eye. Res. (2007), doi:10.1016/j.exer.2007.05.005

which strain could lead to tissue degeneration and the ultrastructural changes of the ONH observed in glaucoma have been proposed, and are supported by evidence about the effects of strain and stress on the load-bearing connective fibres (Hernandez, 1992; Morrison et al., 1990; Quigley et al., 1991a,b), capillaries and on the axons of the RGCs, astrocytes and endothelial cells (Hernandez et al., 1989; Morrison et al., 1990), as recently reviewed by Burgoyne et al. (2005).

Mechanical strain is a measure of deformation, and can be interpreted as the change in length of a material region (e.g. a cell) divided by the resting length of that region. Studies have shown that strain is an important mechanobiological factor that causes effects in many cell types (Bandak, 1995; Edwards et al., 2001; LaPlaca et al., 2005; Pedersen and Swartz, 2005; Tan et al., 2006; Triyoso and Good, 1999; Vossoughi and Bandak, 1995; Wang and Thampatty, 2006). Strain is usually reported as a single value, e.g. ''the cells were strained by 5%''. The situation is more complex than this simple description would imply, however. Cells and tissues can deform in different ways, or ''modes'', such as extension, compression or shearing, although these modes of strain are not independent of one another, as described in more detail in the Appendix. This is not merely a matter of semantics, as it has been established that the mechanobiologic response of tissues (Bain and Meaney, 2000; Edwards et al., 2001) and cells (LaPlaca et al., 2005; Morrison et al., 2005; Pedersen and Swartz, 2005; Tan et al., 2006; Wang and Thampatty, 2006) depends on the mode of deformation (extension, compression or shearing), as well as the magnitude and temporal profile of the stimulus, and the type of tissue or cell and its biological state. It is therefore of interest to determine which modes of strain the tissues of the ONH are exposed to as IOP is elevated.

As IOP changes, different regions of the ONH deform by different amounts and therefore experience different amounts of strain. Even within a single tissue region (e.g. the lamina cribrosa), the strain can vary substantially from location to location. Previously, our group (Sigal et al., 2004, 2005a,b) and others (Bellezza et al., 2000) have simply used mean and peak values of strain to describe the distribution of strain. These quantities, while useful, do not fully describe the strain distribution, and there is a need to better characterize how strains are distributed in various tissue regions.

Strain does not occur within tissues without accompanying stress, which is a measure of the force being carried by the tissue. More specifically, stress is the force in a tissue region divided by the cross-sectional area over which that force acts, and high levels of stress can lead to mechanical failure (tearing) of connective tissue components. For example, Burgoyne has suggested that elevated stresses might cause collagen fibrils in the lamina cribrosa to fail, thereby contributing to optic nerve head remodelling in glaucoma (Burgoyne et al., 2005). It is therefore of interest to quantify the stress distribution in ONH tissues. As is the case for strain, there are different modes of stress, and we will examine the relative magnitudes of these modes throughout the ONH.

The objective of this work was to analyze this previously overlooked aspect of the biomechanical response of an ONH to increases in IOP: the spatial and volumetric distribution of different modes of strain. We found that compressive strains were the dominant mode of strain found in the lamina cribrosa.

2. Materials and methods

Experimental measurements of the biomechanical environment of the ONH are extremely challenging. We therefore employ a standard engineering technique known as finite element modeling (FEM) that allows the biomechanics of the ONH to be simulated while accounting for the geometric complexity of the relevant tissue regions (Meakin et al., 2003; Stay et al., 2005; Viceconti et al., 2006).

2.1. The models

We used finite element methods to predict strains in individual-specific and generic models of human ONHs. The methodology for reconstructing 3D individual-specific models of human ONHs suitable for finite element modeling has been previously reported (Sigal et al., 2005b). Briefly, model geometry was based on serial histologic sections through the ONH of donor eyes fixed at either 5 or 50 mmHg. From each of three donors, one eye was randomly selected for reconstruction. Donor information is provided in Table 1. Eyes were obtained and managed in accordance with the provisions of the declaration of Helsinki for research involving human tissue. Sagittal sections through the ONH were stained and photographed, and then aligned using fiducial markers. Through manual segmentation in Amira 3.1.1 (Mercury Computer Systems Inc, USA) five tissue regions were defined on each section: lamina cribrosa (LC), pre and post-laminar neural tissue, pia mater and peripapillary sclera, and 3D surfaces delimiting each of the tissue regions were constructed (Table 1). The interiors of the regions were volume-meshed and the models ported to Ansys v8.1 (Ansys Inc. Canonsburg, PA, USA) for finite element modeling (Fig. 1). Initially the models were formed by linear 4-node tetrahedral elements (SOLID45 in Ansys), but upon importing into the finite element software the elements were converted into quadratic 10-node tetrahedral elements (SOLID92) and midside nodes added. To ensure mesh independence, all models were meshed to the level of refinement identified as suitable in a previous study (Sigal et al., 2005b).

For comparison, a generic axisymmetric model was also used. This generic model was similar to that described previously (Sigal et al., 2005b), but instead of being based on Model 1 was based on Model 3 (both described in detail in Sigal et al., 2004). Model 3 improves upon Model 1 in that it incorporates the pia mater and more detailed geometry for the cup, the scleral canal and the peripapillary sclera. ''Virtual histologic sections'' were generated from the known geometry of Model 3 and segmented to create this generic model, which was solved and analyzed identically to the individual-specific models.

Please cite this article in press as: Ian A. Sigal et al., Predicted extension, compression and shearing of optic nerve head tissues, Exp. Eye. Res. (2007), doi:10.1016/j.exer.2007.05.005

Table 1
Summary of donor and model properties

	Donor/Model	1	2	3	Generic
	Eye	OS	OD	OD	–
	Age (years)	83	79	91	–
	Gender	M	M	M	–
	Time to enucleation (h)	2	2	10	–
	Time to imaging (h)	17	23.5	29	–
	Fixation pressure (mmHg)	5	5	50	–
Volume (μl)	Pia mater	1.05	1.41	1.61	0.35
	Pre-laminar neural tissue	2.73	2.21	2.80	2.07
	Post-laminar neural tissue	5.49	4.99	5.72	4.03
	Sclera	1.54	1.76	1.97	1.52
	Lamina cribrosa	0.62	0.49	1.08	0.88
	Region of interest	11.42	11.86	13.19	8.85
	Total reconstructed	15.87	15.23	18.60	30.18
Region of interest (ROI)	LC centroid X (μm)	72.6	−27.3	20.2	23.9
	LC centroid Y (μm)	−230.4	−223.0	−227.1	95.5
	LC centroid Z (μm)	−7.8	−92.8	2.7	3.7
	Area LC-Ret (mm^2)	2.75	3.13	4.05	2.86
	Area LC-ON (mm^2)	3.59	3.60	4.62	3.72
	Equivalent radius r_a (μm)	935	998	1136	954
	ROI radius r_b (μm)	1403	1497	1703	1431

Eyes were randomly selected to be fixed at low (5 mmHg) or high (50 mmHg) IOP. All models were simulated for a change in IOP of 45 mmHg. Tissue volumes are within the region of interest, except total volume that corresponds to the whole reconstructed volume. The LC centroid location is with respect to the axis of symmetry of the model used for boundary conditions. The axis of symmetry corresponds to the Y axis, in the anterior-posterior direction. Also shown are the areas of the anterior LC surfaces (LC-Ret) used to compute the equivalent radii, and the posterior LC surfaces (LC-ON) that provide an idea of the variability in the measures and the shape of the LC.

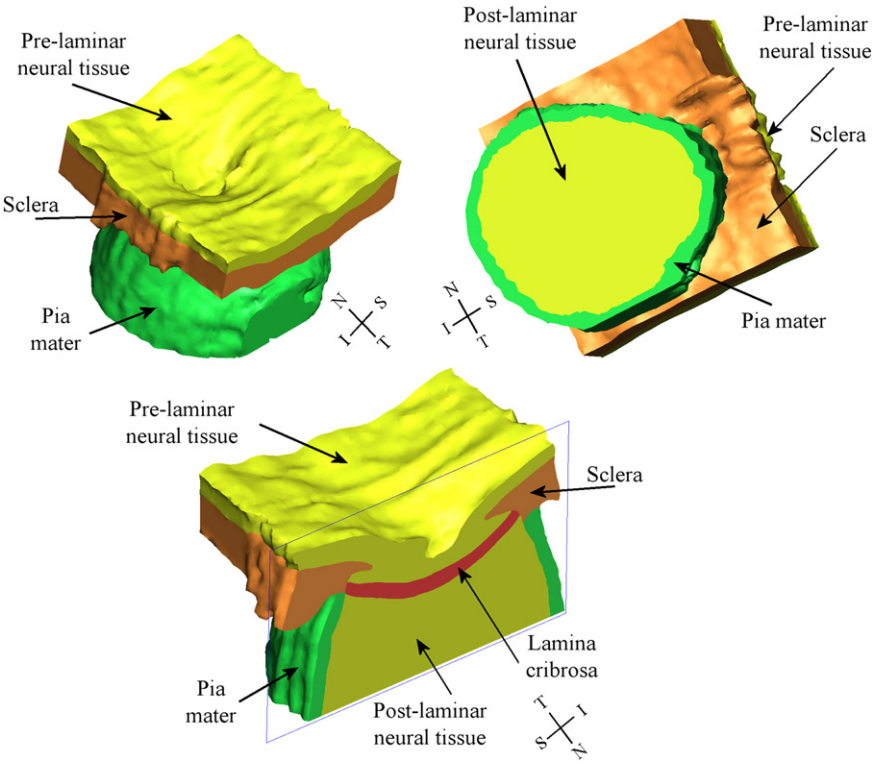

Fig. 1. Example model reconstructed from the OD of Donor 2. The top two panels show the geometry viewed from the anterior (left) and posterior (right); in the bottom panel the model has been cut sagittally through the center of mass to show the interior. The pre-laminar neural tissue includes the retina. The post-laminar neural tissue forms the optic nerve. The lamina cribrosa spans the scleral canal opening and is visible posterior to the cup. S – Superior, I – Inferior, T – Temporal and N – Nasal.

Please cite this article in press as: Ian A. Sigal et al., Predicted extension, compression and shearing of optic nerve head tissues, Exp. Eye. Res. (2007), doi:10.1016/j.exer.2007.05.005

In all models, only the ONH region was reconstructed, and it was therefore necessary to apply boundary conditions to the edges of the models. This was accomplished by embedding the individual-specific models into a generic spherical shell, which was generated by rotating the 2D version of Model 3 around its axis of symmetry (Sigal et al., 2004). Displacements computed from this shell were applied to the edges of the ONH region model. IOP was applied as a force acting on the surfaces of the elements exposed to the interior of the eye. Boundary conditions (displacements on the model edges and the forces representing IOP) were adjusted such that models reconstructed from eyes fixed at 5 mmHg were inflated, i.e. experienced a simulated increase in IOP to 50 mmHg, while those models from eyes fixed at 50 mmHg were "deflated", i.e. experienced a simulated decrease in IOP to 5 mmHg. No other forces or displacements were applied to the models, although the IOP-induced deformations predicted for the axisymmetric model used for boundary conditions were zeroed on the vitreo-retinal interface 5° from the axis of symmetry, as described previously (Sigal et al., 2004, 2005a,b).

Tissue mechanical properties were assigned as for the baseline models (Sigal et al., 2005a). All tissues were modeled as homogeneous, isotropic, and virtually incompressible ($\nu = 0.49$), with a Young's modulus of 3 MPa for the sclera and pia mater, 0.3 MPa for the lamina cribrosa and 0.03 MPa for the pre and post-laminar neural tissues. These assumptions are considerable simplifications, the implications of which will be examined in the Section 4.

Solutions were obtained using ANSYS v8.1 PCG solver with default parameters, typically requiring less than one hour of CPU time on a desktop workstation with Windows XP SP1, an Intel 3.0 GHz CPU and 4 GB of memory.

2.2. Post-processing

The presentation of all results was standardized to show the effects of an increase in IOP from 5 to 50 mmHg, which simplified comparison between eyes. Solutions were exported from ANSYS to Amira using custom scripts, and Amira's node-based plotting was used to yield smooth contour plots (Sigal, 2006). The ANSYS finite element software computed the three principal strains and the three principal stresses, at each node and at the centroid of each element. The principal strains completely describe the magnitude of the strain field at every location in the tissue, while the principal stresses describe the stress field (Cook, 1995). Physically, ε_1, the first principal strain, represents the maximum stretching that a tissue element will experience, while ε_3, the third principal strain, represents the maximum compression that a tissue element will experience. Analogously, the first principal stress represents the maximum extensional force the tissue is subjected to, while the third principal stress represents the maximum compressive force the tissue is subjected to.

From the principal strains, we computed the maximum shear strain:

$$\varepsilon_{\text{shear}} = \frac{1}{2}\left(\varepsilon_1 - \varepsilon_3\right).$$

where ε_1 and ε_3 are the first and third principal strains. To simplify comparison between the various modes of stress and between the various modes of strain, the absolute value of the measure was used in the plots described in the following subsections. However, the use of the absolute value was limited to the display, and all calculations were done using the actual values. To help interpret the plots, it is useful to recall that for an incompressible, or nearly incompressible, material, the first principal strain is positive (extensile) and the third principal strain is negative (compressive).

2.3. Finding percentiles

A combination of standard and custom routines was used to compute the distribution of each strain mode in each tissue region, and from these distributions the 50th and 95th percentile values were computed, representing the median and peak. Defining the peak value as the 95th percentile limited the effects of outliers that could be due to numerical effects (e.g. meshing), or due to approximations introduced during model geometry reconstruction, and which might not represent physiologic effects. Note that this is slightly different from the approach used previously (Sigal et al., 2005a), due to technical differences in the software packages used. Herein the distributions were computed based on the volume exposed to a given level of strain, rather than on the number of elements.

2.4. Defining a region of interest (ROI)

The size of histologic sections from which the ONH model was created and the length of the optic nerve varied from eye to eye. To fairly compare results between models it was necessary to reduce variation as much as possible. We therefore defined a region of interest (ROI) whose volume was adjusted to the LC of each ONH model at 5 mmHg (Table 1), using the methodology described in Fig. 2. Only elements within the ROI (as defined by their centroidal position) were considered for the analysis of distributions (median and peak values) of the strain fields. Elements outside the ROI were not deleted in order to make illustrations clearer.

3. Results

Different measures of strain and stress were plotted on cross sections through an individual-specific model (Fig. 3) and a generic model of the ONH (Fig. 4). For all models, there were substantial differences in the magnitudes and distribution of the various modes of strain. Considering the modes of strain that have a simple physical interpretation, the largest strain magnitudes occurred in compression (third principal strain), followed by shear and finally by extension (first principal strain). The middle (second principal) strain was much smaller than other modes of strain. As expected the stresses were of a smaller magnitude within the more compliant tissues, and

Please cite this article in press as: Ian A. Sigal et al., Predicted extension, compression and shearing of optic nerve head tissues, Exp. Eye. Res. (2007), doi:10.1016/j.exer.2007.05.005

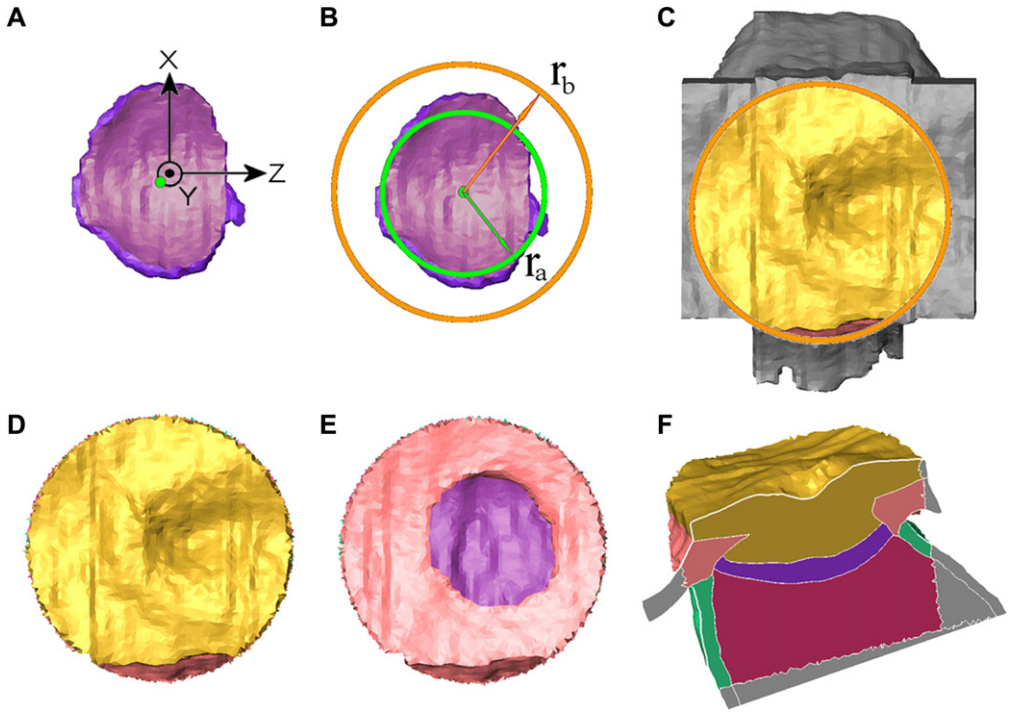

Fig. 2. Diagram of the process for defining the region of interest (ROI). (A) An en face view of the LC of the OS of Donor 1 is shown in purple, from which the center of mass (centroid) of the LC was determined (green dot). The axis of symmetry used for boundary conditions corresponds to the Y axis, not necessarily passing through the LC centroid. (B) The area of the interface between the LC and the pre-laminar neural region was computed, and a disc with the same surface area (equivalent radius, r_a) was overlain on the LC (green line). The radius of the ROI (r_b) was then defined as one and a half times r_a, and also overlain on the LC (orange line). (C) An en face view of the full model of the OS of Donor 1, with the circle defining the ROI boundary shown in orange. (D) Same view as in panel C, but with only the ROI elements shown. (E) Same view as D, but with the pre-laminar neural tissue removed to show sclera (pink), the opening of the scleral canal and the LC behind. (F) Oblique view of the full model, cut sagittally through the center of mass. Elements outside the ROI are grey, those inside are: the pre-laminar neural tissue in yellow, the LC in purple, the post-laminar neural tissue in red, the pia mater in cyan, and the sclera in pink. The posterior limit to the ROI is a plane 1.5 mm posterior to the center of mass of the LC.

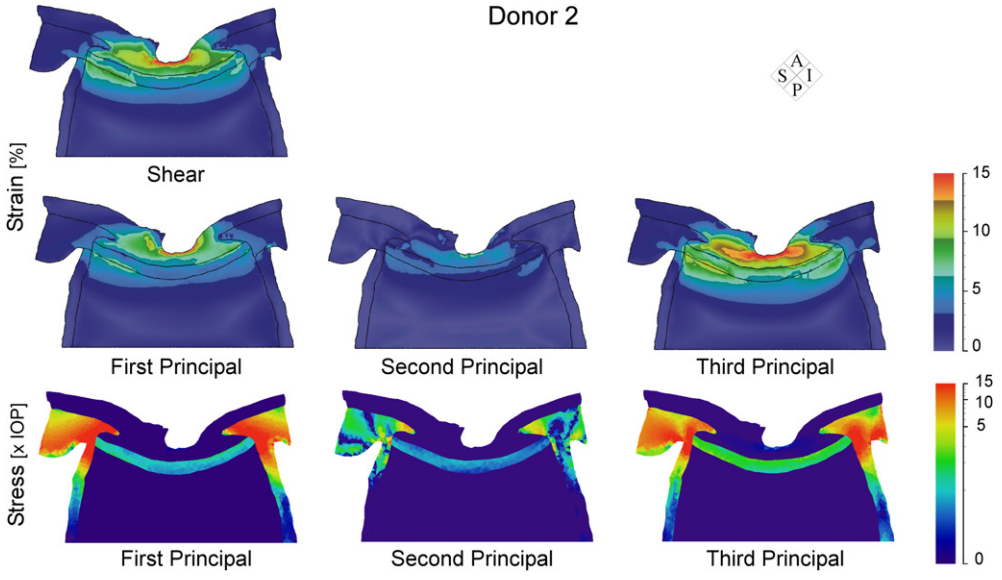

Fig. 3. Comparison of four measures of strain and three measures of stress for one eye. All images are the same sagittal cross section through the center of the OD eye of Donor 2, differing only in the measure represented in the contour levels. The plotted strains and stresses were the result of an increase in IOP from 5 to 50 mmHg. The three principal strains/stresses are the elements of the diagonal of diagonalized strain/stress tensor, ordered from most positive (first), to most negative (third). The shear strain is derived from the principal strains. Clearly visible are the differences in magnitude between the different modes and the non-symmetrical distributions. The magnitude of the stresses varies over several orders of magnitude, hence we used a non-linear (logarithmic) scale for stress, expressed as a multiple of the imposed IOP. To simplify comparison between modes, the absolute value of the measure is shown. The outlines of the tissue regions are shown in black. A – Anterior, P – Posterior, S – Superior, I – Inferior.

Please cite this article in press as: Ian A. Sigal et al., Predicted extension, compression and shearing of optic nerve head tissues, Exp. Eye. Res. (2007), doi:10.1016/j.exer.2007.05.005

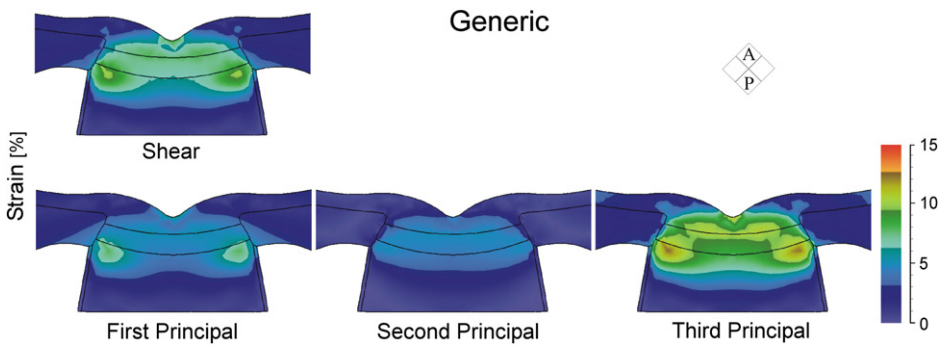

Fig. 4. Comparison of four measures of strain, analogous to those shown in Fig. 3, but for the Generic Model, a 3D reconstruction of the model used for boundary conditions and as the baseline for the parametric and sensitivity analysis previously described (Sigal et al., 2005a). As in the individual-specific model of Fig. 3, the various strain measures differed in their magnitude, but not surprisingly, for this model were highly symmetrical. To simplify comparison between modes of strain the absolute value of the measure is shown. The outlines of the tissue regions are shown in black. A – Anterior, P – Posterior.

larger for relatively stiff regions, with stresses being particularly large in the scleral and pial regions directly adjacent to the LC.

A better understanding of the spatial distribution can be obtained from a series of parallel cross sections (Fig. 5) rather than the single sections shown in Figs. 3 and 4. Regions of higher strain were present in the laminar and neural tissue, as was seen in the single sagittal section. However, looking at the changes in contour levels from one section to another, we notice the complexity of the mechanical response of an ONH to an increase in IOP, such as the concentration of strains in the peripheral post-laminar neural tissue near the LC, the pia mater and the sclera. Each individual-specific geometry could potentially produce completely different strain fields. This will be further analyzed (Sigal, 2006).

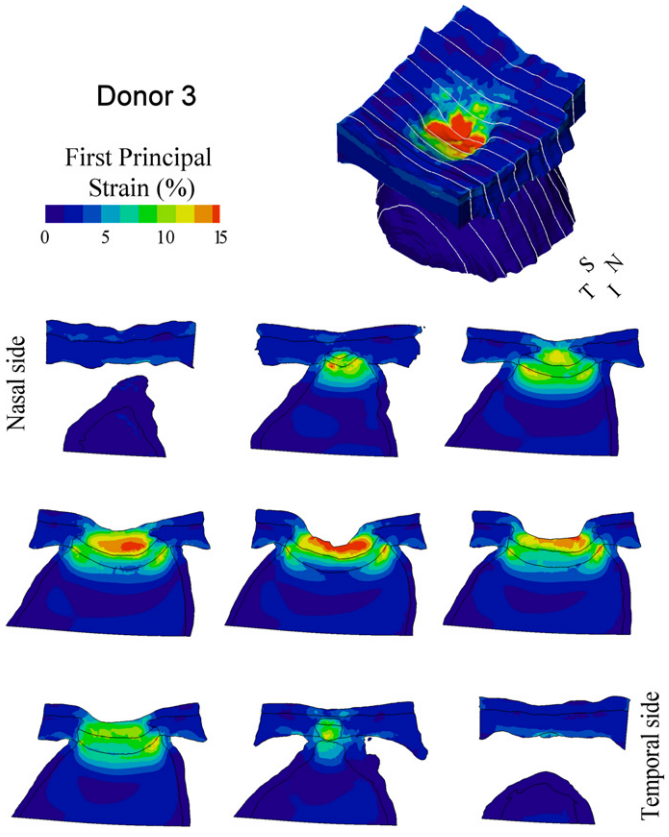

Fig. 5. Spatial distribution of first principal strain on a model reconstructed from the OD of Donor 3. On the top right is an external view of the model. White lines are the locations of the sagittal cross sections shown below, which progress from the nasal (top left) to the temporal side (bottom right). The sections were equally separated with their location determined from the overall size of the ONH models, based on the dimensions of a box that completely enclosed the model. Sections were then taken at 10%, 20%, … 50% (the central section), … 80%, and 90% from one side to the other. On the sagittal sections the inferior side is on the right. S – Superior, I – Inferior, T – Temporal, N – Nasal.

Quantitative analyses of the distribution of strain in an individual-specific model are shown in Figs. 6 and 7. These figures discard the spatial information in favour of aggregated measures of the tissue volume subjected to a given level of strain. The volume integral distribution plots (Fig. 6, right column) reveal that the volume of post-laminar neural tissues subjected to high strain (above 10% compression) was about the same as of laminar tissue. However, the relative fraction plots (Fig. 6, left column) show that a smaller fraction of post-laminar neural tissue than of laminar tissue was subjected to high strain. Surprisingly, there was much more neural than laminar tissue – both in absolute volume and in fraction – subjected to high levels of compressive and shearing strains.

A ‘‘strain histogram’’ for the LC is shown in Fig. 7, which describes the volume of tissue subjected to a given level of strain. Since the three curves are from the same LC, the area under the lines is the same (the volume of the LC), but differences in distribution between the various strain modes are clearly seen. Specifically, there are higher median and peak values (arrows on the X axis) for the third principal strain (compression) when compared with the first principal strain (extension) and the maximum shearing strain (shear). Similar results were obtained for other models. This indicates that the most ‘‘extreme’’ strains that LC tissue experiences are compressive, followed by shear and then extension.

4. Discussion and conclusions

Three main results have been obtained from this work: First, elevation of IOP causes the tissues of the ONH to be subjected to a complex strain environment, characterized by

Please cite this article in press as: Ian A. Sigal et al., Predicted extension, compression and shearing of optic nerve head tissues, Exp. Eye. Res. (2007), doi:10.1016/j.exer.2007.05.005

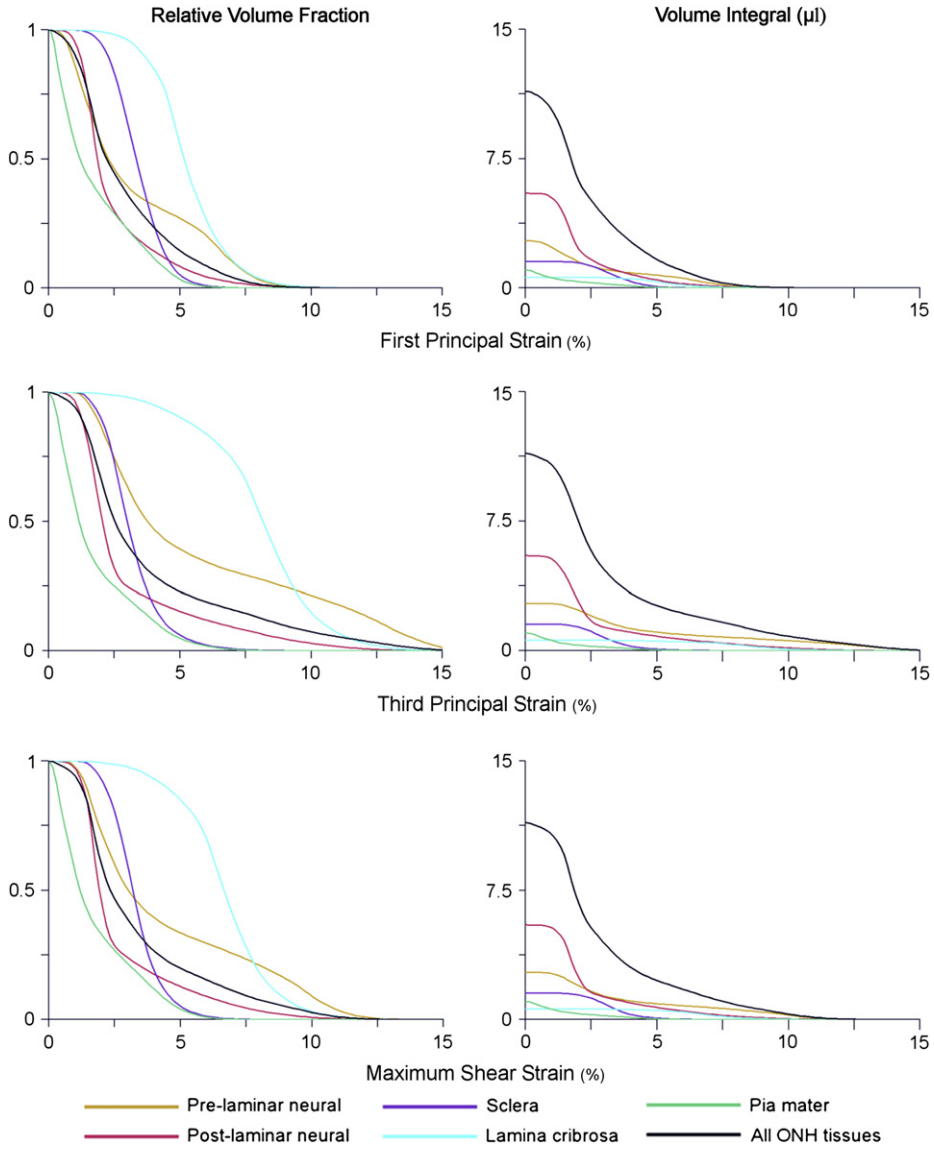

Fig. 6. Cumulative volume distributions of first principal strain (extension; top), third principal strain (compression; middle) and maximum shear strain (bottom) within the ONH tissues of the OS of Donor 1. In the right column, the curves show the volume of tissue that has a strain level greater than or equal to the value on the X axis. The volume of each region is therefore the intersect of the tissue line with the Y axis (strain level = 0). The left column shows similar plots, where the Y-axis values have been scaled by the volume of the tissue they represent. These graphs therefore show the *fraction* of tissue that has a level of strain greater than or equal to the value on the X axis.

multiple modes of strain (extension, compression and shearing) whose magnitude and distribution vary through the ONH. Second, the highest magnitudes of all modes of strain occurred within the neural tissue regions, not within the lamina cribrosa. Third, the largest strain magnitudes were in compression, followed by shearing and finally by extension. The fact that maximum shearing strain has magnitude intermediate between that of first and third principal strains is a consequence of the definition for shearing strain, but nonetheless if of interest since shearing strain has frequently been mentioned in the literature as being potentially very important in retinal ganglion cell loss in glaucoma (Burgoyne et al., 2005; Edwards et al., 2001; Hernandez, 2000; Levy and Crapps, 1984; Yan et al., 1994). Since the stresses are linearly related to strains (although with a different constant of proportionality – i.e. Young's modulus – in each tissue region), the relative proportions of the principal strains in each tissue region match the relative proportions of the stresses in that region.

What is the biological significance of these results? Experiments on neurons and astrocytes have established that mechanical stimulation of a cell has different effects depending on the mode, magnitude and temporal profile of the stimulus (Ellis et al., 1995; Hernandez, 2000; Morgan, 2000; Neufeld et al., 1999; Ostrow et al., 2000). Most in vitro systems for mechanostimulation of astrocytes and neural tissues have subjected cells to stretching (Kirwan et al., 2005). Our work suggests that more refined models are needed that investigate how different strain modes affect biological function of ONH

Please cite this article in press as: Ian A. Sigal et al., Predicted extension, compression and shearing of optic nerve head tissues, Exp. Eye. Res. (2007), doi:10.1016/j.exer.2007.05.005

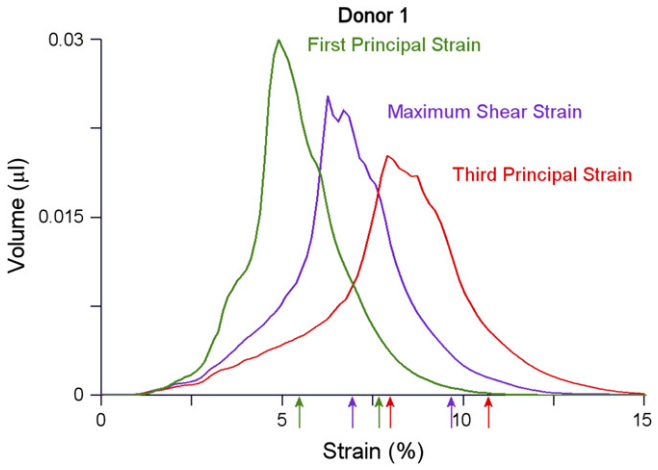

Fig. 7. Distribution of three modes of strain within the lamina cribrosa of the OS eye of Donor 1. The plotted quantity is the volume of LC tissue that experiences the level of strain shown on the X axis. The arrows on the X axis point to the median and peak levels (50th and 95th percentiles) of each distribution. The differences in distribution between the three strain modes are evident. In particular, the distributions of the different modes are clearly not just a scaling up or down of one another. The three curves represent frequencies in the LC of the same eye, and therefore the area below the curve is the same for all: the volume of the LC.

cells. Only when such data are available will it be possible to unequivocally determine whether predicted levels of IOP-induced strain are physiologically relevant.

The complex strain environment within the ONH was in part an outcome of the material properties assumed for the tissues: when effectively incompressible materials are extended in one direction, they must compress in another direction, and vice versa. This effect has been observed in other organs, for example in the spinal cord (Henderson et al., 2005), and has been used to subject cells cultured on a flat plate to 3D deformation (Morrison et al., 2006). For compressible materials the effects of a deformation in one direction on other directions are somewhat dampened, but still occur. Nevertheless, compressibility is not the only mode of transfer of deformations from one direction onto others, as this might still occur due to the structure of the material, as in fibrous tissues (Pedersen and Swartz, 2005).

The existence of simultaneous modes of strain on the ONH tissues was not as surprising as the relative magnitudes of the modes of strain. In the case of an thin-walled elastic sphere inflated by a uniform pressure, it can be shown (under certain assumptions (Timoshenko and Goodier, 1970)) that the first and second principal strains are positive and have the same magnitude, while the third principal strain is negative and has double the magnitude of the other two principal strains. The situation within the ONH is quite different, with a state known as plane strain being approximated, in which one principal strain is negligible (Timoshenko and Goodier, 1970). This shows that the biomechanical environment in the ONH is complex, due to the geometry of the different tissue regions and their differences in material properties, and that it can be difficult to predict the biomechanics of this tissue region by analogy with the biomechanics of a spherical shell.

In our previous analyses of ONH biomechanics we had selected the maximum principal strain (stretching) as the measure of deformation in response to changes in IOP, arguing that it would be a good representation of the deformation that could lead to physiological responses (Sigal et al., 2004, 2005a,b). Others have chosen to compute the principal vector magnitude or the von Mises strain (Bellezza et al., 2000; Bellezza, 2002; Burgoyne et al., 2005; Downs et al., 2004). All these approaches have substantial limitations because they discard information about the true complexity of the strain field, although they are still more informative than literature reports that neglect to describe the type of strain considered, or that confuse one mode with another.

By considering a homogeneous LC, the models presented here cannot account for the effects of the laminar microstructure. The complex geometry of the lamina trabeculae has been hypothesized to amplify the levels of strain, so that the cells attached to the matrix of the LC could be subject to strains several orders of magnitude larger than those of the larger scale structure (Burgoyne et al., 2005). This hypothesis has received support from initial numerical models that considered the laminar micro-structure (Downs et al., 2004), and studies of load transfer in fibrous materials (Pedersen and Swartz, 2005). This could be an explanation as to why the damage to the RGCs seems to occur in the LC, as proposed in glaucoma (Quigley, 2005; Shields, 1997), even though the highest magnitudes of strain were predicted in the neural tissue regions. It is also possible that the RGC axons are not equally sensitive to, or equally capable of recovering from, mechanical stimulation in all regions of the ONH. However, it is also possible that the large differences in stiffness between load-bearing and non-load-bearing (RGC axons and astrocytes for example) tissues have the opposite effect, and instead shield the laminar astrocytes from the large strains of the ECM. Whether the in vivo situation is one of amplification or shielding, or a combination, depends on the composition and microarchitecture of the LC. Studies that consider in detail a realistic laminar micro-structure are necessary to find the answer.

The results presented here are subject to several limitations arising from the process of reconstructing the models, and how IOP increase was simulated and its effects analyzed. Issues regarding the process of reconstructing the models have been discussed previously (Sigal et al., 2005b). For simulation, important assumptions were made about the mechanical properties of the tissues modeled, namely that they were linearly elastic, incompressible, homogeneous and isotropic. Evidence suggests that these are only approximations, and that the mechanical response of the tissues is non-linear (Downs et al., 2005; Spoerl et al., 2005; Woo et al., 1972). Certainly, the tissues are non-homogeneous, being composed in a large fraction by load-bearing collagenous tissues. However, the mechanical properties of the tissues of the ONH are not completely known, and although some recent studies have added to our knowledge of the properties of the ONH tissues (Downs et al., 2003, 2005; Spoerl et al., 2005), we believe that assuming linear material properties provides a reasonable first approximation that allows an improved understanding of ONH

Please cite this article in press as: Ian A. Sigal et al., Predicted extension, compression and shearing of optic nerve head tissues, Exp. Eye. Res. (2007), doi:10.1016/j.exer.2007.05.005

biomechanics. Finally, we recognize that all of the human eyes that we have used were, by necessity, post mortem tissue, and we cannot exclude the possibility of some necrotic changes. In particular, since the sclera is the major determinant of ONH biomechanics, one should be most concerned about scleral changes. There is data that suggests that mechanical properties of the sclera do not change up to 72 h post mortem, at least in rabbit eyes (Girard et al., 2004). This would suggest that scleral geometry would also not change 17–29 h post mortem (the range of post mortem times used in this study), and we therefore feel that the use of post mortem human eyes is reasonable for purposes of this study.

It has been suggested that differences in ONH geometry between individuals could lead to differences in the ONH biomechanical response and sensitivity to elevated IOP (Burgoyne et al., 2005; Jonas et al., 2003, 2004; Quigley and Addicks, 1981; Quigley et al., 1981, 1990). Although there were differences between the predicted responses to changes in IOP between the models used in this work, all four models led to the same conclusions. The effects of differences in ONH geometry on ONH biomechanics are described in detail elsewhere (Sigal, 2006).

Finally, a region of interest (ROI) was defined for each model based on the area of the anterior surface of the LC. Although reasonable, this selection was arbitrary and it is possible that future comparisons between models will require a different definition.

Even considering these limitations, the questions raised by this work remain: what modes of strain have physiologic relevance in each tissue? What distribution analysis is useful to assess the physiologic relevance? How meaningful are the median and peak values? Do we need to know the fraction of tissue that is subject to a certain mode of strain or is it necessary to determine the absolute size of the region that is above a certain threshold? How can we properly compare the mechanical response of two ONHs? We suggest that, while these questions are being answered, the best alternative is to track several measures of strain. In this way, when in the future our understanding of these questions improves, the predictions from these studies will still be relevant.

Considering all possible modes of strain, however, adds significant complexity to the analysis, and ideally a subset of the strain measures shown here would suffice. We suggest focusing attention on the three measures with a clear physical interpretation: first (maximum) principal strain, third (minimum) principal strain, and maximum shearing strain. The second (middle) principal strain is also potentially interesting, however as it was found to be generally of a much smaller magnitude than the first and third principal strains. Other quantities derived from the strain tensor, like the von Mises equivalent strain or the principal vector magnitude, do not have a clear physical interpretation, and therefore are not recommended.

Acknowledgments

This work was supported by the Consejo Nacional de Ciencia y Tecnologia de Mexico (IAS), the Canadian Institutes for Health Research (CRE, JGF), the Canada Research Chairs Program (CRE) and Glaucoma Research Society of Canada. We thank the Eye Bank of Canada for providing donor tissue.

Appendix A

Here we provide a brief overview of the engineering concept of strain. Interested readers are referred to (Humphrey, 2006; Timoshenko and Goodier, 1970) for more details. Strain is a measure of deformation, and is defined as the fractional elongation of a small line-shaped tissue element, i.e. the change in length divided by the original length of that tissue line. A positive strain represents an increase in length, or extension; and a negative strain represents a decrease in length, or compression.

Unfortunately, this simple definition hides a significant complication: in a real-life situation, the magnitude of the elongation of the line-shaped tissue element depends on the orientation of this line, and the direction of elongation may not coincide with the original orientation of the element (Fig. A1). This shows that the strain actually depends on orientation of the tissue line element under consideration. Luckily, it is always possible to identify a set of preferred, or *principal* directions, such that tissue lines oriented in these directions undergo only a pure elongation or a pure compression. The strains that are identified for such line elements are known as the *principal strains*. For a three-dimensional object, there are in general three such principal strains: ε_1, ε_2, and ε_3. By definition, $\varepsilon_1 > \varepsilon_2 > \varepsilon_3$. In an incompressible or nearly incompressible material, the *first principal strain* ε_1 must be greater than zero and therefore represents an extension, while the *third principal strain* ε_3 must be less than zero and therefore represents a compression.

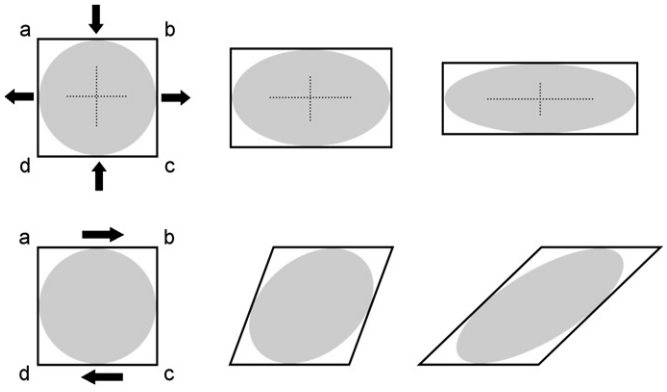

Fig. A1. Schematic illustration of tissue straining in two dimensions. The top row shows an originally square tissue region abcd deformed by forces, represented by the black arrows. Two lines placed on the tissue (see centre of tissue region) elongate or contract, depending on their orientation. This shows that the strain experienced by a line element of tissue depends on the orientation of that line. Superimposed on the square tissue region is a circle that deforms with the tissue. In the bottom row, the same tissue region is sheared. However, this tissue region is also undergoing extension and compression, as can be verified by noting how the length of the imaginary lines ac and bd change. In fact, the ellipses in the final panels of each row are identical, showing that shearing is present in the deformation shown in the top row and elongation/compression is present in the deformation shown in the bottom row.

Please cite this article in press as: Ian A. Sigal et al., Predicted extension, compression and shearing of optic nerve head tissues, Exp. Eye. Res. (2007), doi:10.1016/j.exer.2007.05.005

In addition to extension and compression a material can also undergo shearing. Shearing is the deformation of a tissue line element in a direction other than along the axis of the line (Fig. A1). However, as can be appreciated from Fig. A1, a deformation that appears at first glance to consist of a pure extension in one direction and a pure compression in the orthogonal direction, can actually be interpreted as including a shearing deformation. Similarly, a shearing deformation can be interpreted as including extension and compression. This shows that the modes of strain are not independent of one another, a fact which becomes clearer when we re-examine the definition of the maximum shear strain, which is in fact expressed in terms of principal strains, $\varepsilon_{\text{shear}} = \frac{1}{2}(\varepsilon_1 - \varepsilon_3)$. It is for this reason that we have focussed on the principal strains in this paper, since they are a fundamental representation of the strain field from which the magnitude of other strain measures can be computed.

The reader may therefore ask: why bother reporting the maximum shearing strain? Even though this quantity is directly derived from the first and third principal strains, we include plots of $\varepsilon_{\text{shear}}$ to avoid readers having to mentally compute shearing strain distributions from plots of first and third principal strains, and because researchers in the field of glaucoma have an intuitive understanding of shearing strain that is reflected in many discussions of the possible pathologic role of this quantity in mechanically insulting retinal ganglion cell axons in the lamina cribrosa (Burgoyne et al., 2005; Edwards et al., 2001; Hernandez, 2000; Levy and Crapps, 1984; Yan et al., 1994).

References

Bain, A.C., Meaney, D.F., 2000. Tissue-level thresholds for axonal damage in an experimental model of central nervous system white matter injury. J. Biomech. Eng. 122 (6), 615–622.

Bandak, F.A., 1995. On the mechanics of impact neurotrauma: a review and critical synthesis. J. Neurotrauma 12 (4), 635–649.

Bellezza, A.J., Hart, R.T., Burgoyne, C.F., 2000. The optic nerve head as a biomechanical structure: initial finite element modeling. Invest. Ophthalmol. Vis. Sci. 41 (10), 2991–3000.

Bellezza, A.J., 2002. Biomechanical Properties of the Normal and Early Glaucomatous Optic Nerve Head: an Experimental and Computational Study Using the Monkey Model. Department of Biomedical Engineering, Tulane University.

Burgoyne, C.F., Downs, J.C., Bellezza, A.J., Suh, J.K., Hart, R.T., 2005. The optic nerve head as a biomechanical structure: a new paradigm for understanding the role of IOP-related stress and strain in the pathophysiology of glaucomatous optic nerve head damage. Prog. Retin. Eye Res. 24 (1), 39–73.

Cook, R.D., 1995. Finite Element Modeling for Stress Analysis. John Wiley & Sons, Inc.

Downs, J.C., Suh, J.K., Thomas, K.A., Bellezza, A.J., Burgoyne, C.F., Hart, R.T., 2003. Viscoelastic characterization of peripapillary sclera: material properties by quadrant in rabbit and monkey eyes. J. Biomech. Eng. 125 (1), 124–131.

Downs, J.C., Hart, R.T., Grau, V., Bellezza, A.J., Hirons, B.A., Burgoyne, C.F., 2004. Micro Finite Element Modeling of the Lamina Cribrosa in Monkey Eyes. E-Abstract 2157. ARVO, Ft. Lauderdale, FL, USA.

Downs, J.C., Suh, J.K., Thomas, K.A., Bellezza, A.J., Hart, R.T., Burgoyne, C.F., 2005. Viscoelastic material properties of the peripapillary sclera in normal and early-glaucoma monkey eyes. Invest. Ophthalmol. Vis. Sci. 46 (2), 540–546.

Edwards, M.E., Wang, S.S., Good, T.A., 2001. Role of viscoelastic properties of differentiated SH-SY5Y human neuroblastoma cells in cyclic shear stress injury. Biotechnol. Prog. 17 (4), 760–767.

Ellis, E.F., McKinney, J.S., Willoughby, K.A., Liang, S., Povlishock, J.T., 1995. A new model for rapid stretch-induced injury of cells in culture: characterization of the model using astrocytes. J. Neurotrauma 12 (3), 325–339.

Girard, M., Downs, J.C., Suh, J.K., Hart, R.T., Burgoyne, C.F., Downs, J.C., 2004. Effects of Storage Time on The Mechanical Properties of Rabbit Peripapillary Sclera after Enucleation. E-Abstract 2177. ARVO, Ft. Lauderdale, FL, USA.

Henderson, F.C., Geddes, J.F., Vaccaro, A.R., Woodard, E., Berry, K.J., Benzel, E.C., 2005. Stretch-associated injury in cervical spondylotic myelopathy: new concept and review. Neurosurgery 56 (5), 1101–1113. discussion 1101–1113.

Hernandez, M.R., Luo, X.X., Andrzejewska, W., Neufeld, A.H., 1989. Age-related changes in the extracellular matrix of the human optic nerve head. Am. J. Ophthalmol. 107 (5), 476–484.

Hernandez, M.R., 1992. Ultrastructural immunocytochemical analysis of elastin in the human lamina cribrosa. Changes in elastic fibers in primary open-angle glaucoma. Invest. Ophthalmol. Vis. Sci. 33 (10), 2891–2903.

Hernandez, M.R., 2000. The optic nerve head in glaucoma: role of astrocytes in tissue remodeling. Prog. Retin. Eye Res. 19 (3), 297–321.

Humphrey, J.D., 2006. Cardiovascular Solid Mechanics. Springer.

Jonas, J.B., Berenshtein, E., Holbach, L., 2003. Anatomic relationship between lamina cribrosa, intraocular space, and cerebrospinal fluid space. Invest. Ophthalmol. Vis. Sci. 44 (12), 5189–5195.

Jonas, J.B., Berenshtein, E., Holbach, L., 2004. Lamina cribrosa thickness and spatial relationships between intraocular space and cerebrospinal fluid space in highly myopic eyes. Invest. Ophthalmol. Vis. Sci. 45 (8), 2660–2665.

Kirwan, R.P., Fenerty, C.H., Crean, J., Wordinger, R.J., Clark, A.F., O'Brien, C.J., 2005. Influence of cyclical mechanical strain on extracellular matrix gene expression in human lamina cribrosa cells in vitro. Mol. Vis. 11, 798–810.

LaPlaca, M.C., Cullen, D.K., McLoughlin, J.J., Cargill 2nd, R.S., 2005. High rate shear strain of three-dimensional neural cell cultures: a new in vitro traumatic brain injury model. J. Biomech. 38 (5), 1093–1105.

Levy, N.S., Crapps, E.E., 1984. Displacement of optic nerve head in response to short-term intraocular pressure elevation in human eyes. Arch. Ophthalmol. 102 (5), 782–786.

Meakin, J.R., Shrive, N.G., Frank, C.B., Hart, D.A., 2003. Finite element analysis of the meniscus: the influence of geometry and material properties on its behaviour. Knee 10 (1), 33–41.

Morgan, J.E., 2000. Optic nerve head structure in glaucoma: astrocytes as mediators of axonal damage. Eye 14 (Pt 3B), 437–444.

Morrison, J.C., Dorman-Pease, M.E., Dunkelberger, G.R., Quigley, H.A., 1990. Optic nerve head extracellular matrix in primary optic atrophy and experimental glaucoma. Arch. Ophthalmol. 108 (7), 1020–1024.

Morrison, J.C., Johnson, E.C., Cepurna, W., Jia, L., 2005. Understanding mechanisms of pressure-induced optic nerve damage. Prog. Retin. Eye Res. 24 (2), 217–240.

Morrison 3rd, B., Cater, H.L., Benham, C.D., Sundstrom, L.E., 2006. An in vitro model of traumatic brain injury utilising two-dimensional stretch of organotypic hippocampal slice cultures. J. Neurosci. Methods 150 (2), 192–201.

Neufeld, A.H., Sawada, A., Becker, B., 1999. Inhibition of nitric-oxide synthase 2 by aminoguanidine provides neuroprotection of retinal ganglion cells in a rat model of chronic glaucoma. Proc. Natl. Acad. Sci. USA 96 (17), 9944–9948.

Ostrow, L.W., Langan, T.J., Sachs, F., 2000. Stretch-induced endothelin-1 production by astrocytes. J. Cardiovasc. Pharmacol. 36 (5 Suppl. 1), S274–S277.

Pedersen, J.A., Swartz, M.A., 2005. Mechanobiology in the third dimension. Ann. Biomed. Eng. 33 (11), 1469–1490.

Quigley, H.A., Addicks, E.M., 1981. Regional differences in the structure of the lamina cribrosa and their relation to glaucomatous optic nerve damage. Arch. Ophthalmol. 99 (1), 137–143.

Please cite this article in press as: Ian A. Sigal et al., Predicted extension, compression and shearing of optic nerve head tissues, Exp. Eye. Res. (2007), doi:10.1016/j.exer.2007.05.005

Quigley, H.A., Addicks, E.M., Green, W.R., Maumenee, A.E., 1981. Optic nerve damage in human glaucoma. II. The site of injury and susceptibility to damage. Arch. Ophthalmol. 99 (4), 635–649.

Quigley, H.A., Brown, A.E., Morrison, J.D., Drance, S.M., 1990. The size and shape of the optic disc in normal human eyes. Arch. Ophthalmol. 108 (1), 51–57.

Quigley, H.A., Brown, A., Dorman-Pease, M.E., 1991a. Alterations in elastin of the optic nerve head in human and experimental glaucoma. Br. J. Ophthalmol. 75 (9), 552–557.

Quigley, H.A., Dorman-Pease, M.E., Brown, A.E., 1991b. Quantitative study of collagen and elastin of the optic nerve head and sclera in human and experimental monkey glaucoma. Curr. Eye Res. 10 (9), 877–888.

Quigley, H.A., 2005. Glaucoma: macrocosm to microcosm the Friedenwald lecture. Invest. Ophthalmol. Vis. Sci. 46 (8), 2662–2670.

Shields, B., 1997. Textbook of Glaucoma, fourth ed. Williams & Wilkins, Baltimore.

Sigal, I.A., Flanagan, J.G., Tertinegg, I., Ethier, C.R., 2004. Finite element modeling of optic nerve head biomechanics. Invest. Ophthalmol. Vis. Sci. 45 (12), 4378–4387.

Sigal, I.A., Flanagan, J.G., Ethier, C.R., 2005a. Factors influencing optic nerve head biomechanics. Invest. Ophthalmol. Vis. Sci. 46 (11), 4189–4199.

Sigal, I.A., Flanagan, J.G., Tertinegg, I., Ethier, C.R., 2005b. Reconstruction of human optic nerve heads for finite element modeling. Technol. Health Care 13 (4), 313–329.

Sigal, I.A., 2006. Human Optic Nerve Head Biomechanics: an Analysis of Generic and Individual-Specific Models Using the Finite Element Method. Department of Mechanical and Industrial Engineering, University of Toronto, Toronto.

Spoerl, E., Boehm, A.G., Pillunat, L.E., 2005. The influence of various substances on the biomechanical behavior of lamina cribrosa and peripapillary sclera. Invest. Ophthalmol. Vis. Sci. 46 (4), 1286–1290.

Stay, M.S., Pan, T., Brown, J.D., Ziaie, B., Barocas, V.H., 2005. Thin-film coupled fluid-solid analysis of flow through the Ahmed glaucoma drainage device. J. Biomech. Eng. 127 (5), 776–781.

Tan, J.C., Kalapesi, F.B., Coroneo, M.T., 2006. Mechanosensitivity and the eye: cells coping with the pressure. Br. J. Ophthalmol. 90 (3), 383–388.

Timoshenko, S., Goodier, J., 1970. Theory of Elasticity. McGraw-Hill, New York.

Triyoso, D.H., Good, T.A., 1999. Pulsatile shear stress leads to DNA fragmentation in human SH-SY5Y neuroblastoma cell line. J. Physiol. 515 (Pt 2), 355–365.

Viceconti, M., Pancanti, A., Varini, E., Traina, F., Cristofolini, L., 2006. On the biomechanical stability of cementless straight conical hip stems. Proc. Inst. Mech. Eng. [H] 220 (3), 473–480.

Vossoughi, J., Bandak, F.A., 1995. Mechanical characteristics of vascular tissue and their role in brain injury modeling: a review. J. Neurotrauma 12 (4), 755–763.

Wang, J.H., Thampatty, B.P., 2006. An introductory review of cell mechanobiology. Biomech. Model Mechanobiol. 5 (1), 1–16.

Woo, S.L., Kobayashi, A.S., Schlegel, W.A., Lawrence, C., 1972. Nonlinear material properties of intact cornea and sclera. Exp. Eye Res. 14 (1), 29–39.

Yan, D.B., Coloma, F.M., Metheetrairut, A., Trope, G.E., Heathcote, J.G., Ethier, C.R., 1994. Deformation of the lamina cribrosa by elevated intraocular pressure. Br. J. Ophthalmol. 78 (8), 643–648.

Please cite this article in press as: Ian A. Sigal et al., Predicted extension, compression and shearing of optic nerve head tissues, Exp. Eye. Res. (2007), doi:10.1016/j.exer.2007.05.005